Aalborg Universitet

Transient Monitoring Function–Based Fault Detection for Inverter-Interfaced Microgrids

Sadeghkhani, Iman; Esmail Hamedani Golshan, Mohamad; Mehrizi-Sani, Ali; Guerrero, Josep M.; Ketabi, Abbas

Transient Monitoring Function–Based Fault Detection for Inverter-Interfaced Microgrids

Iman Sadeghkhani, *Graduate Student Member, IEEE,* Mohamad Esmail Hamedani Golshan,
Ali Mehrizi-Sani, *Senior Member, IEEE*, Josep M. Guerrero, *Fellow, IEEE*, and Abbas Ketabi

Abstract—One of the major challenges in protection of the inverter-interfaced islanded microgrids is their limited fault current level. This degrades the performance of traditional overcurrent protection schemes. This paper proposes a fault detection strategy based on monitoring the transient response of the inverter current waveform using a transient monitoring function (TMF). To enhance the ability of the proposed fault detection scheme, an auxiliary control system is employed in addition to the main control system of the inverter. The proposed scheme can also differentiate asymmetrical and symmetrical fault conditions from normal load switching events and is effective for various inverter topologies (i.e., three/four-leg), main current limiting strategies, and all reference frames of the multi-loop control system. The merits of the proposed fault detection scheme are demonstrated through several time-domain simulation case studies using the CIGRE benchmark low voltage microgrid network.

Index Terms—Current limiting, distributed energy resources (DER), fault detection, inverter, microgrid, reference frame, transient monitoring function (TMF), voltage-sourced converter (VSC).

I. Introduction

IN recent years, the paradigm of active distribution systems is being realized by the innovations in the small-scale distributed energy resources (DER) such as microturbines, photovoltaics, wind turbines, fuel cells, and storage devices. The electronically coupled DER (EC-DER) units, commonly interfaced using a voltage-sourced converter (VSC), have been gaining popularity among industries and utilities due to their flexibility in providing controlled and high-quality power to loads and to the grid [1], [2]. Microgrids, as an inherent part of the modern smart grids [3], are an effective solution to alleviate the technical issues associated with high penetration of DERs [4]. A microgrid can operate in either grid-connected or islanded (autonomous) modes, thereby offering increased reliability and efficiency to the end user [5], [6].

Fault current values vary significantly between grid-connected and islanded modes of operation [7], [8]. In the grid-connected mode, the fault current flowing from the host grid is comparatively large, which can easily trigger the operation of conventional overcurrent relays [4], [9]. The main challenge arises in the islanded mode of operation in which the fault current contribution of EC-DERs is relatively small. This is due to the fact that during short-circuit faults, the inverter current is typically limited to 2–3 times the rated current, mainly using a current limiting strategy embedded in the inverter control system [10], to prevent damage to semiconductor switches [11]. This condition is very different from the case of a synchronous machine, which generates fault currents 4–10 times the rated current [12]. Consequently, traditional relays may be ineffective for detecting the lower fault currents produced by the EC-DERs [13].

One of the main requirements of a protection scheme is to detect fault conditions. Common fault detection methods in microgrids employ three electrical features: (1) voltage waveform features, (2) voltage or current symmetrical components, and (3) differential quantities. The first group works mainly based on either the network voltage drop in the microgrid [14], [15] or the distortion in voltage waveform during a fault [16]. The former may maloperate during any voltage drop while the latter is not reliable because the inverter voltage waveform is not necessarily distorted for all fault conditions [10]. Harmonic distortion of current is also used in [17], [18] to detect fault conditions. The second category of fault detection schemes usually works based on the zero-sequence current for grounding fault types and the negative-sequence current for double line faults [19]. These strategies can not detect a symmetrical fault and their performance are degraded due to the inherent unbalanced nature of distribution networks.

To address the shortcomings of the first and second fault detection categories, multifeature fault detection schemes are proposed [4], [11]. Reference [11] proposes a fault detection strategy for voltage- and current-controlled VSCs in which unbalanced faults are detected by measuring the symmetrical components while three-phase faults are detected using the overcurrent/undervoltage protection scheme. Also, [4] employs network-wide voltage drop, instantaneous overcurrent relay, and symmetrical components of the current to detect solid and medium-impedance faults.

The third category schemes measure differential features to detect various fault conditions. The main features are the differential current [7] or the differential energy [20]. The latter is less sensitive to synchronization errors than the former. An impedance differential method is proposed in [21] to identify the fault instant. Through analysis of several differential features including RMS values, total harmonic distortion (THD),

I. Sadeghkhani and M. E. Hamedani Golshan are with the Department of Electrical and Computer Engineering, Isfahan University of Technology, Isfahan 84156-83111, Iran (email: i.sadeghkhani@ec.iut.ac.ir; hgolshan@cc.iut.ac.ir).

A. Mehrizi-Sani is with the Energy Systems Innovation Center and the School of Electrical Engineering and Computer Science, Washington State University, Pullman, WA 99164-2752 USA (e-mail: mehrizi@eecs.wsu.edu).

J. M. Guerrero is with the Institute of Energy Technology, Aalborg University, Aalborg 9220, Denmark (email: joz@et.aau.dk).

A. Ketabi is with the Department of Electrical Engineering, University of Kashan, Kashan 87317-51167, Iran (email: aketabi@kashanu.ac.ir).

and symmetrical components of the voltage and current as well as power factor angles, [13] shows that the differential symmetrical components of current show the best performance in detecting faults. Unlike the first and second categories that use local features, a differential protection scheme needs a communication infrastructure.

The effects of inverter topology (three/four-leg), current limiting strategy, and adopted reference frame on the performance of a fault detection scheme constitute the motivation of this work as they are not fully addressed yet. This paper proposes a fault detection strategy for EC-DERs using only the local information. By monitoring the inverter current using a transient monitoring function (TMF), the proposed fault detection scheme can detect the transition from normal to fault operating conditions. Moreover, the proposed fault detection scheme uses the data obtained from the VSC control system. Specifically, the objectives of this paper are as follows:

- To investigate the effects of adopted reference frame, employed current limiting strategy, and inverter topology on the performance of two of the most used local fault detection schemes;
- To identify a local feature for fault detection that is effective for various fault conditions; and
- To distinguish a fault condition from load switching.

This paper is organized as follows. Section II describes the DER control structure. The effects of inverter control system and topology on the two of the most used local fault detection schemes are studied in Section III. Section IV is dedicated to the proposed fault detection scheme. Section V presents the CIGRE low voltage (LV) benchmark microgrid network, which is used in the simulation case studies of Section VI to evaluate the performance of the proposed strategy. Finally, Section VII concludes the paper.

II. DER CONTROL STRATEGY

During the autonomous mode of operation of a microgrid, the frequency and voltage are not externally imposed by the main grid. In this case, at least one voltage-controlled VSC is required to regulate the voltage and frequency at the DER terminal. The VSC control system is usually implemented using a multi-loop control structure [22], [23], as shown in Fig. 1. The control system includes an outer voltage control loop and an inner current control loop. The former regulates the voltage across the filter capacitance C_f by calculating the inductor current reference i_L^{ref} for the current control loop. The droop method is used to calculate the voltage reference v_o^{ref} for the voltage controller. By controlling the current of the filter inductor L_f, the inner control loop improves the power quality. The current limiter block in the output of the voltage controller limits the inductor current reference to approximately 2–3 times the rated current to protect the inverter semiconductor switches [9]. These control loops can be implemented in the synchronous reference frame (SYRF or $dq(0)$ coordinates), stationary reference frame (STRF or $\alpha\beta(\gamma)$ coordinates), or natural reference frame (NARF or abc coordinates) [24]. As the DC link capacitor between the primary source and the inverter is large, the DC output voltage
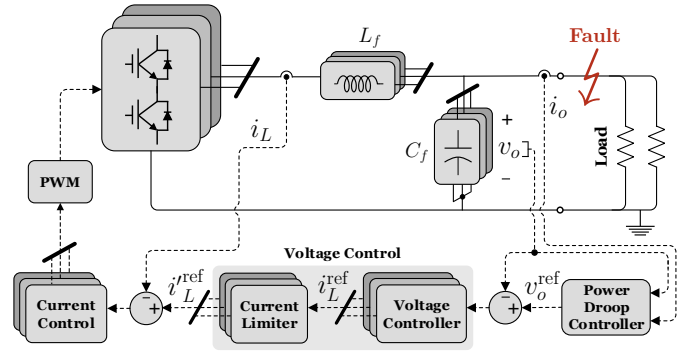

Fig. 1. Basic structure of DER control.

remains almost constant during short transients; therefore, it is common to assume a constant DC input voltage [25].

III. EFFECT OF VSC CONTROL SYSTEM AND TOPOLOGY ON FAULT DETECTION

Due to the low thermal inertia of VSCs, their current should be limited during fault conditions [9], [26]. There are three main current limiting strategies for VSCs: instantaneous saturation, latched, and hybrid reference frame limitings. Limiting strategy, inverter topology, and reference frame of the control system play an important role in fault studies [10]. This section investigates the effect of these factors on two of the most used local fault detection schemes: (1) symmetrical components–based method and (2) THD-based method.

A. Instantaneous Saturation Limiting (ISL) Strategy

In the ISL strategy, the inductor current reference in each axis is limited as

$$i'^{\text{ref}}_L = \begin{cases} i_{\text{th}}, & i_L^{\text{ref}} > i_{\text{th}} \\ -i_{\text{th}}, & i_L^{\text{ref}} < -i_{\text{th}} \\ i_L^{\text{ref}}, & \text{otherwise}, \end{cases} \tag{1}$$

where i_{th} is the current threshold in the limiting strategy, which is adopted 2 pu in this work.

Both network characteristics and VSC control system affect the magnitude and behavior of the fault current. Table I shows the effect of the ISL strategy on the negative- and zero-sequence components as well as the THD of output voltage and current of VSC during various fault conditions across the load in Fig. 1. The example test system of Fig. 1 is a three-phase 380 V, 50 Hz islanded system which includes a 10 kVA VSC and two parallel 3 kW resistive loads. The simulation results are obtained in different reference frames for both three- and four-leg inverters equipped with ISL strategy. The simulated faults are line-to-ground (L-G), double line-to-ground (L-L-G), line-to-line (L-L), and three-phase line-to-ground (L-L-L-G). Symmetrical components–based fault detection schemes usually employ the zero-sequence component of the VSC current for detecting ground faults while they use the negative-sequence component of this current for detecting two-phase faults. It is clear that the zero-sequence component is not available in the current of a three-wire system because
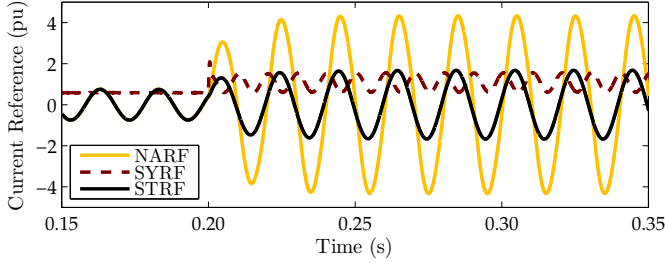
Fig. 2. Unlimited inductor current reference for a three-leg VSC during a single-phase to ground fault. The fault occurs at $t = 0.2$ s.

there is no path (neutral wire) for this component. Thus, the zero-sequence component of the voltage should be employed for detecting ground faults in three-wire systems. Moreover, symmetrical components–based fault detection schemes can not detect symmetrical faults. On the other hand, since control in each reference frame is performed in the specific coordinates, the values of negative- and zero-sequence components are different in various fault conditions, as shown in Table I. For example, during an L-G fault when using a three-wire VSC, the negative sequence component of voltage for NARF is 0.27 pu while it is zero for SYRF and STRF. On the other hand, during the same fault condition, the negative sequence components of current for SYRF and STRF are 0.54 pu and 0.58 pu, respectively, while this component is zero for NARF. Such behavior makes it difficult to design a reliable symmetrical components–based fault detection scheme.

Additionally, as the ISL strategy clips the crest of the sinusoidal current reference during overcurrent conditions, the VSC output voltage and current waveforms are distorted. This distortion can be used as a feature for fault detection. The threshold for fault detection using THD of voltage is 8% as stated in IEEE standard 519 for systems with voltage levels lower than 1.0 kV [27]. As shown in Table I, THD-based fault detection schemes can detect most fault conditions. However, since clipping a DC signal yields another DC signal, these schemes fail to detect symmetrical faults in SYRF case. During unbalanced faults in the SYRF case, the current reference is clipped due to having a sinusoidal ripple occurring at twice the nominal frequency. Consequently, these faults can be detected by the THD-based fault detection scheme. Moreover, THD-based fault detection schemes fail to detect single-phase to ground faults in the SYRF and STRF cases in three-wire systems. Such systems either are not grounded or are grounded in a single point. In the first case, the fault current does not flow during single-phase to ground faults while in the second case, the fault current may not be large enough to exceed the current threshold. Unlike the SYRF/STRF case in which the control system does not include the zero-sequence component, this component of output voltage enters the voltage controller in the NARF case and increases the inductor current reference, as shown in Fig. 2. Thus, the single-phase to ground faults in the NARF case can be detected by a THD-based fault detection scheme due to crest clipping of the current reference.

B. Latched Limiting (LL) Strategy

In this method, during a fault, the inductor current reference is replaced by a predefined current reference vector. This strategy is expressed in (2a) for the NARF case and in (2b) for the SYRF and STRF cases:

$$i'^{\text{ref}}_{L,j} = \begin{cases} i^{\text{lat}}_{L,j}, & I^{\text{ref}}_{L,j} > i_{\text{th}}/\sqrt{2} \\ i^{\text{ref}}_{L,j}, & \text{otherwise} \end{cases} ; \; j = a, b, c \quad (2a)$$

$$\overrightarrow{i}'^{\text{ref}}_{L,dq(0)/\alpha\beta(\gamma)} = \begin{cases} \overrightarrow{i}'^{\text{lat}}_{L,dq(0)/\alpha\beta(\gamma)}, & |\overrightarrow{i}'^{\text{ref}}_{L,dq(0)/\alpha\beta(\gamma)}| > i_{\text{th}} \\ \overrightarrow{i}'^{\text{ref}}_{L,dq(0)/\alpha\beta(\gamma)}, & \text{otherwise}, \end{cases}$$

$$(2b)$$

where I^{ref}_L is the RMS value of the inductor current reference, and i^{lat}_L is the predefined current reference. Because the NARF case provides independent control of each phase, i^{ref}_L is replaced by i^{lat}_L only in the faulted phase(s), as described in (2a). Equation (2b) shows that during various fault types, the same current reference is applied in SYRF/STRF case.

Table II presents the effects of LL strategy on the main features of local fault detection schemes during various fault types. As a predefined current reference is employed during faults, no clipping occurs and consequently the THD-based fault detection schemes fail to detect most fault types. During a single-phase to ground fault in the NARF case for a three-wire system, the predefined current reference is employed only in the faulty phase and the current references in other two phases are produced by the voltage controller. Thus, the zero-sequence component of voltage increases the current reference. This current reference can not be tracked by the current controller because the inverter current is not high during a single-phase to ground fault, as discussed in Subsection III-A. Consequently, the voltage and current waveforms are distorted and the THD-based fault detection schemes can detect only this fault type. On the other hand, different values of symmetrical components of output voltage and current are again observed in various reference frames, as shown in Table II. Moreover, the predefined current reference developed by the LL strategy results in a different behavior of the symmetrical components as compared to the case of using ISL strategy with the clipped current reference (Table I).

C. Hybrid Reference Frame Limiting (HRFL) Strategy

To address the drawbacks of ISL and LL strategies in limiting function, the HRFL strategy is proposed in [10]. In this strategy, during overcurrent conditions, the inductor current reference in the NARF case is reduced by a current limiting factor (CLF) as

$$i'^{\text{ref}}_{L,j} = \text{CLF}_j \times i^{\text{ref}}_{L,j}; \; j = a, b, c, \quad (3)$$

where

$$\text{CLF}_j = \begin{cases} \dfrac{i_{\text{th}}}{\sqrt{2} \times I^{\text{ref}}_{L,j}}, & I^{\text{ref}}_{L,j} > \dfrac{i_{\text{th}}}{\sqrt{2}} \\ 1, & \text{otherwise}. \end{cases} ; \; j = a, b, c. \quad (4)$$

To preserve the voltage magnitude controllability in healthy phase(s) in the SYRF and STRF cases, the main control system is replaced by an auxiliary control system implemented in

TABLE I
EFFECTS OF ISL STRATEGY ON THE MAIN FEATURES OF LOCAL FAULT DETECTION SCHEMES

| Frame | Fault Type | Three-Wire Configuration | | | | | | Four-Wire Configuration | | | | | |
| | | Symmetrical Components (pu) | | | | THD (%) | | Symmetrical Components (pu) | | | | THD (%) | |
		V^-	V^0	I^-	I^0	THD_V	THD_I	V^-	V^0	I^-	I^0	THD_V	THD_I
NARF	L-G	0.27	0.34	0	0	59.2	59.1	0.33	0.33	0.61	0.61	23.0	23.0
	L-L-G	0.32	0.31	0.98	0	29.9	29.9	0.33	0.33	0.62	0.60	25.6	23.0
	L-L	0.40	0	1.16	0	30.0	30.0	0.45	0	1.13	0	57.1	23.3
	L-L-L-G	0	0	0	0	20.0	17.7	0	0	0	0	28.7	23.1
SYRF	L-G	0	0.95	0.54	0	0.67	0.56	0.29	0.22	1.15	1.23	28.9	28.9
	L-L-G	0.23	0.23	1.21	0	38.9	36.2	0.12	0.12	0.57	1.25	39.2	39.2
	L-L	0.24	0	1.29	0	20.0	36.2	0.32	0	1.30	0	28.7	37.9
	L-L-L-G	0	0	0	0	0.89	0.89	0	0	0	0	0.95	0.92
STRF	L-G	0	0.98	0.58	0	0.45	0.45	0.48	0	0.86	1.14	11.9	11.8
	L-L-G	0.59	0.59	1.11	0	13.5	27.8	0.24	0.24	0.61	1.38	35.5	35.5
	L-L	0.64	0	1.14	0	11.6	28.7	0.64	0	1.14	0	6.15	28.6
	L-L-L-G	0	0	0	0	29.2	26.5	0	0	0	0	26.2	26.1

TABLE II
EFFECTS OF LL STRATEGY ON THE MAIN FEATURES OF LOCAL FAULT DETECTION SCHEMES

| Frame | Fault Type | Three-Wire Configuration | | | | | | Four-Wire Configuration | | | | | |
| | | Symmetrical Components (pu) | | | | THD (%) | | Symmetrical Components (pu) | | | | THD (%) | |
		V^-	V^0	I^-	I^0	THD_V	THD_I	V^-	V^0	I^-	I^0	THD_V	THD_I
NARF	L-G	0.44	0.88	0.55	0	12.2	12.2	0.33	0.33	0.47	0.47	0.83	0.83
	L-L-G	0.32	0.32	0.70	0	0.56	1.31	0.33	0.33	0.47	0.47	0.85	0.83
	L-L	0.48	0	0.65	0	1.09	1.82	0.49	0	1.16	0	1.55	4.66
	L-L-L-G	0	0	0	0	1.04	0.61	0	0	0	0	0.89	0.85
SYRF	L-G	0.29	0.73	0.28	0	0.37	0.37	0.62	0.61	0.56	0.56	0.70	0.69
	L-L-G	0.89	0.88	0.61	0	0.48	1.14	0.61	0.61	0.56	0.56	0.89	0.70
	L-L	1.11	0	0.75	0	0.51	1.16	0.92	0	0.84	0	0.37	0.77
	L-L-L-G	0	0	0	0	1.71	0.85	0	0	0	0	1.63	0.63
STRF	L-G	0.58	0.97	0.40	0	0.55	0.55	0.72	0.72	0.49	0.49	1.01	1.01
	L-L-G	0.81	0.80	0.56	0	0.19	1.38	0.72	0.72	0.49	0.49	0.89	0.89
	L-L	1.0	0	0.69	0	0.44	1.57	1.09	0	0.74	0	0.88	0.88
	L-L-L-G	0	0	0	0	1.03	0.98	0	0	0	0	1.86	0.65

NARF during overcurrent conditions. Therefore, the behavior of the studied features in the presence of HRFL strategy are the same in all reference frames, as shown in Table III. However, different values of symmetrical components, compared to the cases of using ISL and LL strategies, show the importance of considering the effect of the VSC control system in a reliable symmetrical components–based fault detection scheme. Moreover, due to proper limiting of the current reference, no distortion appears and THD-based fault detection schemes fail to detect all fault conditions.

IV. PROPOSED FAULT DETECTION STRATEGY

The study presented in Section III shows that symmetrical components–based fault detection schemes suffer from (1) inability in detecting symmetrical faults and (2) different behavior of symmetrical components of voltage and current when using various current limiting strategies, reference frames, and inverter topologies. Moreover, the inherent unbalanced nature of the distribution networks can lead to malfunction of this method [2]. THD-based fault detection schemes can not detect the following fault conditions either: (1) all fault types when using the HRFL strategy, (2) most fault types when using the LL strategy, and (3) single-phase to ground faults in SYRF and STRF cases in a three-leg VSC and symmetrical faults in the SYRF case for both three- and four-leg VSCs when using the ISL strategy.

To address these limitations, this paper employs a transient monitoring function [28] in which the input signal is monitored and any changes in its form is quickly detected. Fig. 3 shows a moving data window for a VSC current waveform before and during a fault condition for which TMF is computed. The length of the window is a key parameter affecting the performance of this approach; a longer window increases

TABLE III
EFFECTS OF HRFL STRATEGY ON THE MAIN FEATURES OF LOCAL FAULT DETECTION SCHEMES

Frame	Fault Type	Three-Wire Configuration						Four-Wire Configuration					
		Symmetrical Components (pu)				THD (%)		Symmetrical Components (pu)				THD (%)	
		V^-	V^0	I^-	I^0	THD_V	THD_I	V^-	V^0	I^-	I^0	THD_V	THD_I
NARF	L-G	0.33	0.33	0	0	0.47	0.47	0.33	0.34	0.47	0.46	1.57	1.57
	L-L-G	0.33	0.33	0.70	0	0.33	0.59	0.33	0.33	0.48	0.46	1.70	1.61
	L-L	0.50	0	0.86	0	0.32	0.64	0.46	0	0.87	0	1.45	1.44
	L-L-L-G	0	0	0	0	0.54	0.54	0	0	0	0	1.66	1.39
SYRF	L-G	0.25	0.41	0	0	0.79	0.79	0.33	0.33	0.47	0.47	1.31	1.31
	L-L-G	0.34	0.33	0.63	0	0.70	1.11	0.33	0.33	0.47	0.47	1.51	1.40
	L-L	0.53	0	0.74	0	0.58	1.31	0.46	0	0.87	0	0.78	0.89
	L-L-L-G	0	0	0	0	1.06	1.06	0	0	0	0	1.66	1.39
STRF	L-G	0.33	0.33	0	0	1.29	1.29	0.33	0.33	0.47	0.47	1.34	1.34
	L-L-G	0.33	0.33	0.69	0	0.79	1.36	0.33	0.33	0.47	0.46	1.51	1.40
	L-L	0.49	0	0.85	0	0.68	1.30	0.46	0	0.87	0	0.76	0.89
	L-L-L-G	0	0	0	0	1.34	1.34	0	0	0	0	1.71	1.44

Fig. 3. Moving data window on a VSC current waveform.

Fig. 4. The actual and reconstructed signals of a VSC current waveform.
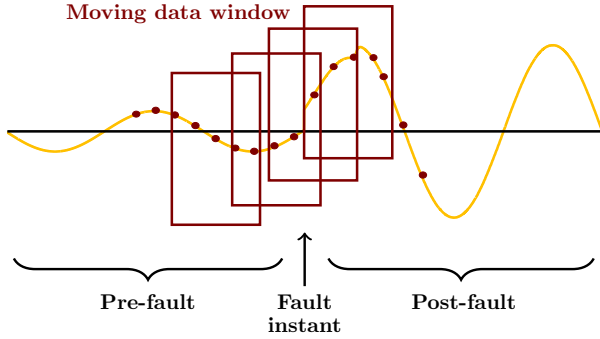
the accuracy but decreases the response time and process speed. In the first step, the fundamental frequency component of the VSC current waveform is estimated using the least square (LS) method [28]. During normal conditions, the actual signal and its reconstruction from the estimated fundamental component match. As shown in Fig. 4, when a fault occurs, the inverter current changes instantaneously, which causes deviation from the reconstructed signal due to the following: (1) in the fault instant, the related windows contain both pre- and post-fault data, as shown in Fig. 3 and (2) the added components to the fault current owing to fault occurrence are not available in the defined model of the signal in the LS approach. Consequently, by defining a proper TMF, this transition from normal operation to faulty condition can be detected. The mathematical description of LS-based TMF is described in the remainder of this section.

A. Transient Monitoring Function

Consider the measured VSC current signal to be processed as
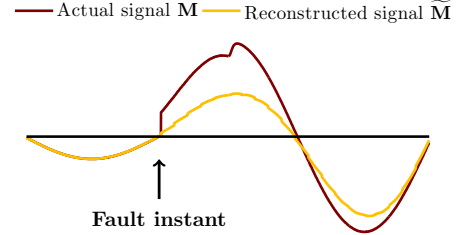
$$i(t) = \sum_{n=1}^{2N} c_n s_n(t), \tag{5}$$

where N is the maximum harmonic order of the signal. $s_n(t)$ are known signals and c_n are the unknown coefficients. The common choices for the signals $s_n(t)$ are

$$\mathbf{S} = \begin{bmatrix} s_1 \\ s_2 \\ s_3 \\ s_4 \\ \vdots \end{bmatrix}^\text{T} = \begin{bmatrix} \cos(\omega_0 t) \\ \sin(\omega_0 t) \\ \cos(2\omega_0 t) \\ \sin(2\omega_0 t) \\ \vdots \end{bmatrix}^\text{T} \left. \begin{array}{l} \\ \end{array} \right\} \text{fundamental frequency} \\ \left. \begin{array}{l} \\ \end{array} \right\} \text{second harmonic} \\ \left. \begin{array}{l} \\ \end{array} \right\} \text{other harmonics,} \tag{6}$$

where ω_0 is the fundamental frequency of the VSC current. Thus, (5) can be written as

$$\begin{aligned} i(t) = &\, c_1 \cos(\omega_0 t) + c_2 \sin(\omega_0 t) \\ &+ c_3 \cos(2\omega_0 t) + c_4 \sin(2\omega_0 t) + \dots. \end{aligned} \tag{7}$$

In the first step of the proposed method, the current signal is sampled with a sampling period of T_s. The discrete form of (5) is

$$m_k = \sum_{n=1}^{2N} c_n s_n(kT_s), \tag{8}$$

where m_k is kth component of the current measurement vector $\mathbf{M}$:

$$\mathbf{M} = \begin{bmatrix} i(t_0 + T_s) & i(t_0 + 2T_s) & \dots & i(t_0 + KT_s) \end{bmatrix}^\text{T}, \tag{9}$$

where K is the number of samples within one cycle. Then, the fundamental frequency component of the VSC current is estimated using the LS technique. For this purpose, (8) can be written in vector form as

$$\mathbf{M} = \mathbf{S_1}\mathbf{C_1}, \qquad (10)$$

where $\mathbf{C_1} = \begin{bmatrix} c_1, c_2 \end{bmatrix}^{\mathrm{T}}$ and $\mathbf{S_1}$ is the discrete form of the first two rows of (6):

$$\mathbf{S_1} = \begin{bmatrix} \cos(\omega_0 T_s) & \cos(\omega_0 2T_s) & \ldots & \cos(\omega_0 KT_s) \\ \sin(\omega_0 T_s) & \sin(\omega_0 2T_s) & \ldots & \sin(\omega_0 KT_s) \end{bmatrix}^{\mathrm{T}}. \qquad (11)$$

The LS solution $\widehat{\mathbf{C}}_1$ for the estimation of coefficients is

$$\widehat{\mathbf{C}}_1 = (\mathbf{S_1^T S_1})^{-1} \mathbf{S_1^T M}. \qquad (12)$$

Using (12), the reconstruction of the current samples $\widetilde{\mathbf{M}}$ can be calculated from the estimate $\widehat{\mathbf{C}}_1$ as

$$\widetilde{\mathbf{M}} = \mathbf{S_1}\widehat{\mathbf{C}}_1 = \mathbf{S_1}(\mathbf{S_1^T S_1})^{-1}\mathbf{S_1^T M}. \qquad (13)$$

If $\widetilde{\mathbf{M}}$ is not close to $\mathbf{M}$, it indicates departure from the normal conditions, which is possibly caused by a fault. The difference can be calculated as

$$\mathbf{R} = \widetilde{\mathbf{M}} - \mathbf{M} = \begin{bmatrix} \mathbf{S_1}(\mathbf{S_1^T S_1})^{-1}\mathbf{S_1^T} - \mathbf{I} \end{bmatrix}\mathbf{M}, \qquad (14)$$

where the residual is $\mathbf{R} = \begin{bmatrix} r_1, r_2, \ldots, r_k \end{bmatrix}^{\mathrm{T}}$. TMF is defined as the sum of the absolute values of r_k over one cycle, i.e.,

$$\mathrm{TMF} = \sum_{k=1}^{K} |r_k|. \qquad (15)$$

B. Fault Detection Scheme

The change in the inverter current as a result of a fault causes the reconstructed samples of inverter output current waveform to deviate from their actual values. In such conditions, TMF is large because the data window includes both pre- and post-fault data. To properly detect this transition, the maximum value of TMF among three phases is calculated as

$$d = \max(\mathrm{TMF}_a, \mathrm{TMF}_b, \mathrm{TMF}_c). \qquad (16)$$

Fig. 5 shows the flowchart of the proposed fault detection scheme. A fault condition is verified when $d > d_{\mathrm{th}}$, where d_{th} is the threshold for fault detection. To distinguish a fault condition from a load switching event, d_{th} should be properly selected. A potential challenge is that during a single-phase to ground fault in a three-wire system, the inverter output current does not significantly change which may cause failure of the proposed fault detection scheme. An alternative is to use the inductor current reference for calculating TMF. However, i_L^{ref} in the two-axis SYRF and STRF cases does not significantly increase during this fault type. Thus, d obtained from $i_{L,dq/\alpha\beta}^{\mathrm{ref}}$ is not a reliable feature. This problem is not present when the inverter control system is implemented in NARF because the zero-sequence component of the voltage increases the unlimited inductor current reference significantly. To address this issue, this paper proposes to use a parallel voltage controller implemented in NARF when the main control system is implemented in SYRF/STRF for three-wire
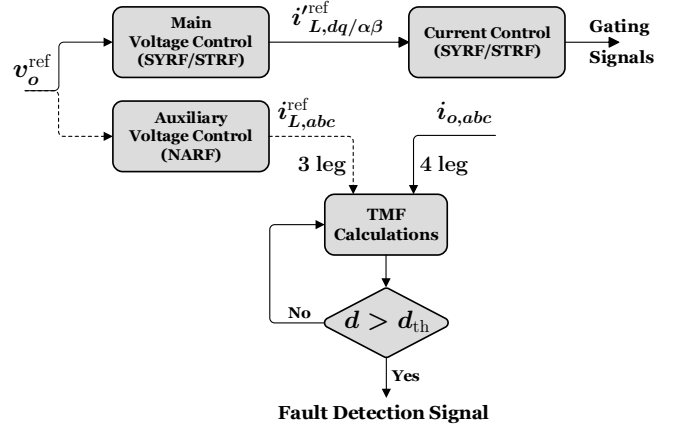

Fig. 5. Flowchart of the proposed fault detection scheme.

systems. As shown in Fig. 5, this auxiliary control system contributes only in providing $i_{L,abc}^{\mathrm{ref}}$ for TMF calculation and does not play any role in producing the switching signals. In the case of using the HRFL strategy, $i_{L,abc}^{\mathrm{ref}}$ is calculated using the parallel voltage control embedded in the control system.

V. STUDY MICROGRID

Fig. 6 shows the single-line diagram of the CIGRE benchmark LV microgrid network [29] as the study system. This system is proposed initially in the EU project "Microgrids," and CIGRE later selected it as a benchmark LV system. The CIGRE benchmark represents common LV (four-wire) distribution feeders with a variety of load types and includes six DER units. The overhead LV feeder serves a suburban residential area. DERs 4 and 5 as well as loads 3 and 7 are single phase. To show the performance of the proposed fault detection scheme in three-wire systems, the CIGRE benchmark LV microgrid is also simulated with three wires. As the three-wire systems usually are balanced, the three-wire CIGRE benchmark LV microgrid is modified as a balanced network, as previously done in [30]. In this study, the control systems of DERs 1, 4, and 5 are implemented in NARF, and the control system of DER 3 is implemented in STRF, with the proportional + resonant voltage controllers as $G_v(s) = k_{pv} + 2k_{rv}\omega_{cv}s/(s^2 + 2\omega_{cv}s + \omega_0^2)$. Also, the controllers of DERs 2 and 6 are implemented in SYRF, with the proportional-integral voltage controllers as $G_v(s) = k_{pv} + k_{iv}/s$. The voltage controllers employ the conditional integration method as the anti-windup strategy in which the difference between i_L^{ref} and $i_L'^{\mathrm{ref}}$ is fed back through the voltage control limiting gain k_{tv} to reduce the error input going to the integrator. All current controllers are implemented using the proportional controllers as $G_i(s) = k_{pi}$. The benchmark data are given in Table IV.

VI. STUDY CASES AND SIMULATION RESULTS

In this section, several case studies are performed to illustrate the performance of the proposed fault detection scheme. The simulation studies for both three- and four-wire configurations of the study microgrid system are performed in MATLAB/Simulink environment. The developed scenarios include
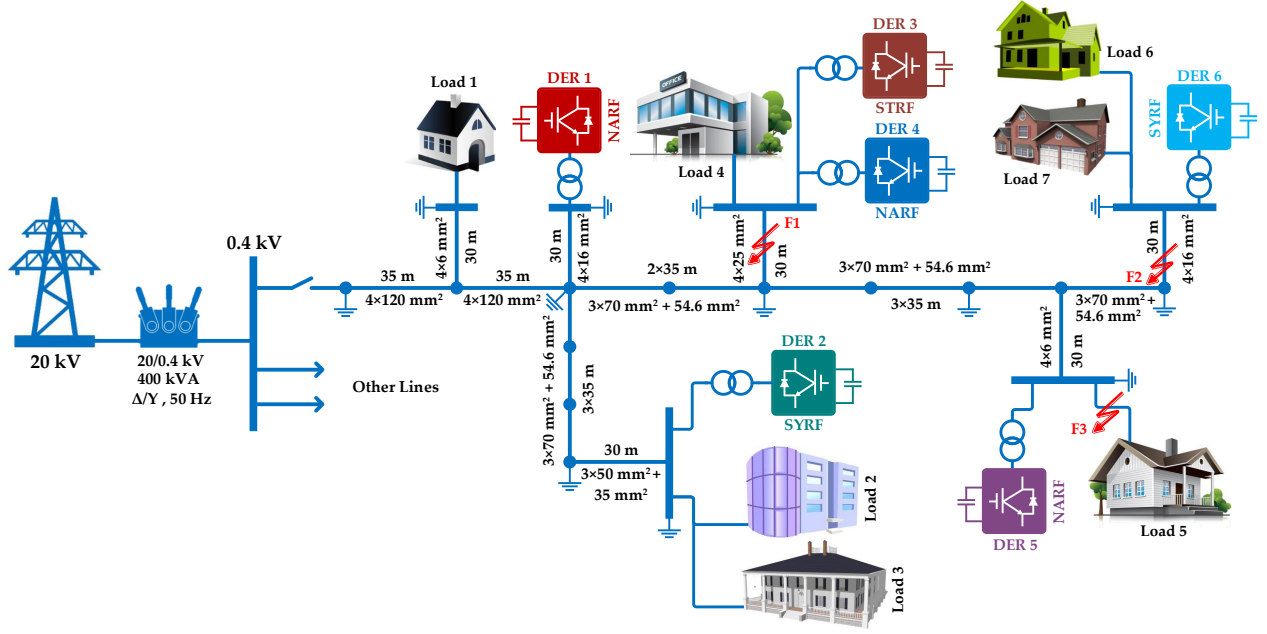
Fig. 6. CIGRE benchmark LV microgrid network.

TABLE IV
CIGRE BENCHMARK LV MICROGRID PARAMETERS

	DER Parameters							
Type	**Parameter**	**Symbol**	**DER 1**	**DER 2**	**DER 3**	**DER 4**	**DER 5**	**DER 6**
Electrical	Rated power	S_n (kVA)	45	45	15	15	5	15
	Rated voltage	V_n (V)	400	400	400	400	400	400
	DC bus voltage	V_{dc} (V)	1000	1000	1000	1000	1000	1000
	Fundamental frequency	f_0 (Hz)	50	50	50	50	50	50
	Switching frequency	f_{sw} (Hz)	5000	5000	5000	5000	5000	5000
	Filter inductance	L_f (mH)	1	1	5	5	5	5
	Filter capacitance (3W*)	C_f (μF)	100	100	30	100	150	30
	Filter capacitance (4W)	C_f (μF)	100	100	30	30	150	30
	Series impedance of the isolating transformer (1:1) at 50 Hz	$\overline{Z}_{eq}$ (Ω)	$0.50 + j1.22$	$0.42 + j1.01$	$0.75 + j1.82$	$0.75 + j1.82$	$0.84 + j2.03$	$0.75 + j1.82$
Droop Control	Real power droop coefficient	m_p	1.84	1.84	5.51	5.51	16.52	5.51
	Reactive power droop coefficient	n_q	0.075	0.075	0.23	0.23	0.68	0.23
	Power calculation cut-off frequency	$\omega_c(\frac{\text{rad}}{\text{s}})$	$2\pi \times 5$	$2\pi \times 5$	$2\pi \times 5$	$2\pi \times 5$	$2\pi \times 5$	$2\pi \times 5$
Control Loops	Voltage control proportional term (3W)	k_{pv}	2	1	2	10	30	1
	Voltage control proportional term (4W)	k_{pv}	2	1	2	2	2	1
	Voltage control proportional term (4W-LL)	k_{pv}	2	1	2	2	30	1
	Voltage control resonant/integral term	k_{rv}/k_{iv}	200	300	200	200	200	300
	Voltage control limiting gain	k_{tv}	0.5	0.5	0.5	0.5	0.5	0.5
	Voltage control cut-off frequency	$\omega_{cv}(\frac{\text{rad}}{\text{s}})$	2	—	2	2	2	—
	Current control proportional term	k_{pi}	1000	100	1000	1000	1000	100

	Load Parameters						
Type	**Parameter**	**Load 1**	**Load 2**	**Load 3**	**Load 4**	**Load 5**	**Load 6**	**Load 7**
Electrical	Rated real power (kW)	5	30	15	20	10	7	13
	Power factor	0.85	0.8	0.8	0.9	0.85	0.8	0.8

*3W and 4W refer to three- and four-wire configurations, respectively.

asymmetrical and symmetrical faults and load switchings at various sections of the test system. The sampling rate of the current signal is 20 samples per 50 Hz cycle, i.e., $T_s = 1$ ms. Table V presents the performance of the proposed TMF-based fault detection method during various solid fault conditions at F1, F2, and F3 in CIGRE benchmark LV microgrid for both three- and four-wire configurations when various current limiting strategies are employed in DER controllers. The DERs have different responses depending on the location and severity of the fault. Detecting the fault condition by at least one DER satisfies the aim of this paper which is the fault detection in the study microgrid. Table V, compared with Tables I–III, shows the effectiveness of the proposed method in detecting all fault conditions. The results of both three-phase and single-phase load switchings are also presented in Table V to show the ability of the proposed fault detection method in differentiating these events from a fault condition.

Adoption of proper threshold plays an important role in the performance of the proposed method. When a transient event occurs, d changes based on the severity of the event. As shown in Table V, d values for the fault conditions are larger than those for the four biggest load switchings. In the cases of load switchings, the maximum value of d for the three-wire system is 4.60 pu while it is only 1.86 pu for the four-wire configuration. Consequently, adopting $d_{\mathrm{th}} = 5$ pu guarantees proper operation of the proposed TMF-based fault detection method for the study system.

Four case studies, 1) two-phase fault at F1, 2) single-phase to ground fault at F2, 3) three-phase to ground fault at F3, and 4) load 2 switching, are investigated with more details as follows. All scenarios start at $t = 2$ s.

A. Case 1: Line-to-Line Fault

The objective of this case study is to evaluate the performance of the proposed fault detection scheme during an asymmetrical fault in the four-wire study microgrid with HRFL strategy employed for all DERs. A two-phase fault is simulated in the middle of the feeder of DER 3 (F1 in Fig. 6). As shown in Fig. 7, the transition from pre-fault to post-fault conditions is detected by d calculated from the output current i_o of DER 3 and it reaches 11.3 pu. The proposed strategy only takes about 2 ms to exceed d_{th}. Due to the action of HRFL strategy, the inverter current is sinusoidal after fault inception instant and consequently d returns to about zero during the fault. For the same fault condition in the three-wire system, d increases to 10.8 pu, as shown in Table V, which confirms the effectiveness of the proposed method in detecting L-L faults for both three- and four-wire configurations.

B. Case 2: Line-to-Ground Fault

This case study evaluates the ability of the proposed scheme for detecting a single-phase to ground fault (F2 in Fig. 6) in the three-wire study microgrid system in which all DERs are equipped with the ISL strategy. Fig. 8 shows the DER 6 output current and d. As the inverter current does not significantly change during this condition, d obtained from i_o reaches only 4.19 pu and does not exceed d_{th}. However, d calculated from
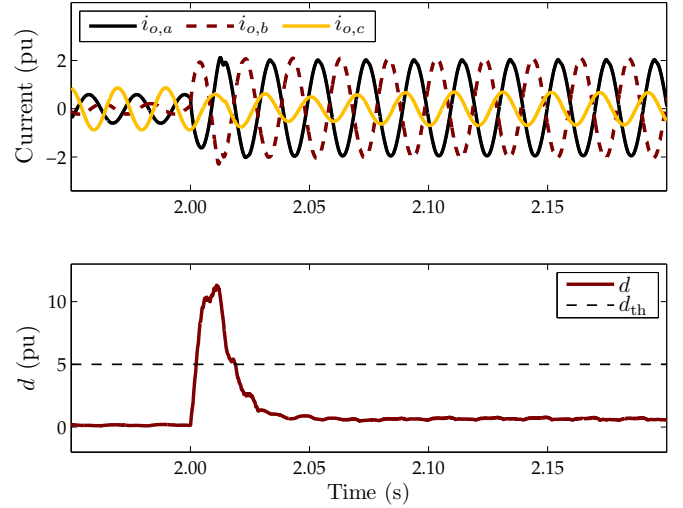

Fig. 7. Output current and d calculated for DER 3 of the study microgrid during an a-b fault. DERs are four-leg and equipped with the HRFL strategy.
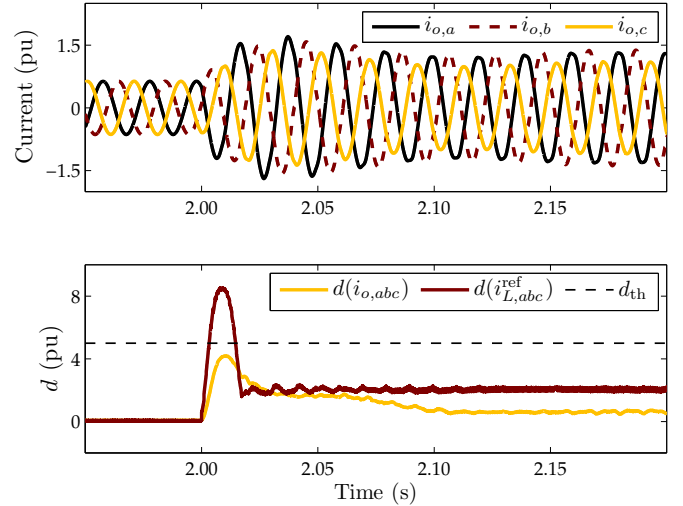

Fig. 8. Output current and d calculated for DER 6 of the study microgrid during an a-g fault. DERs are three-leg and equipped with the ISL strategy.

i_L^{ref} (obtained from the auxiliary voltage control implemented in NARF) increases to about 8.5 pu. The fault detection time for this case study is about 3 ms. It should be noted that the action of ISL strategy distorts the inverter current reference during the fault and the fit of the estimate to the data is not good. Consequently, the magnitude of d does not return to zero, rather it is about 2 pu during the fault. In the case of this fault condition in four-wire configuration, d calculated from i_o exceeds the threshold as it reaches 7.15 pu, as shown in Table V.

C. Case 3: Three-Phase Line-to-Ground Fault

Detection of symmetrical faults is the most challenging problem for local fault detection schemes. To demonstrate the effectiveness of the proposed scheme during these faults, a three-phase line to ground fault is simulated across load 5 (F3 in Fig. 6). In this case, the three-wire study microgrid

TABLE V
PERFORMANCE OF PROPOSED TMF-BASED FAULT DETECTION METHOD FOR CIGRE BENCHMARK LV MICROGRID

Event—Limiter	Type	Three-Wire Configuration						Four-Wire Configuration					
		d_1(pu)	d_2(pu)	d_3(pu)	d_4(pu)	d_5(pu)	d_6(pu)	d_1(pu)	d_2(pu)	d_3(pu)	d_4(pu)	d_5(pu)	d_6(pu)
F1 — HRFL	L-G	14.2	15.6	15.1	36.8	83.0	16.3	8.52	5.57	12.4	7.71	2.14	14.1
	L-L-G	13.3	15.2	15.6	37.5	97.0	17.1	8.51	6.08	11.6	7.68	9.83	8.26
	L-L	7.17	12.0	10.8	24.6	77.9	13.1	7.26	6.00	11.3	4.09	9.85	6.32
	L-L-L-G	9.11	11.4	12.8	28.6	92.0	14.4	8.53	6.75	11.0	7.73	9.87	9.12
F2 — ISL	L-G	15.5	7.27	7.49	37.5	88.2	8.52	7.49	4.91	10.7	6.35	1.69	7.15
	L-L-G	13.1	6.69	7.58	30.0	86.9	8.60	7.45	6.50	10.6	6.34	9.95	10.4
	L-L	6.40	5.07	5.57	19.0	75.2	6.91	6.60	4.74	10.1	3.66	9.79	6.51
	L-L-L-G	8.10	5.33	6.31	24.5	92.2	7.56	7.48	7.59	10.6	6.41	9.97	10.6
F3 — LL	L-G	35.2	28.8	32.1	104	210	27.0	6.56	4.26	35.0	5.54	3.03	5.98
	L-L-G	29.4	13.9	19.8	81.0	211	18.4	6.50	9.15	25.3	5.52	42.3	15.6
	L-L	5.32	9.48	16.1	67.8	84.9	23.9	5.99	4.36	27.5	3.63	15.0	16.5
	L-L-L-G	6.63	8.94	22.6	95.9	220	24.1	6.60	7.73	24.3	5.65	42.7	15.5
Load Switching													
Load 2 – HRFL	3-phase	0.98	1.42	1.14	2.13	4.60	1.37	1.16	1.18	1.42	0.54	1.33	1.15
Load 4 – ISL	3-phase	0.53	0.33	0.39	1.29	2.67	0.40	0.64	0.63	0.83	0.41	0.74	0.77
Load 3 – LL	1-phase	0.49	0.69	0.52	0.98	2.47	0.65	1.44	0.97	1.72	1.04	0.80	0.86
Load 7 – HRFL	1-phase	0.42	0.51	0.47	0.89	2.73	0.74	1.32	1.14	1.86	0.22	0.33	1.65

system is adopted in which all DERs employ the LL strategy. Fig. 9 shows the simulation results for this case study. d calculated from the inductor current reference i_L^{ref} of DER 5 (obtained from the main voltage control which is in NARF) increases to 220 pu and exceeds its threshold after about 1 ms. The high value of d is due to (1) calculating d using the unlimited current reference in three-wire systems, (2) high voltage control proportional term of DER 5 controller, and (3) high current distortion in the first cycles after fault inception. The actual and reconstructed signals match during the fault because the inverter current is sinusoidal and the estimation is properly done. In the four-wire configuration, the proposed method can also detect this fault condition because d calculated from the output current i_o reaches 42 pu, as shown in Table V.

D. Case 4: Three-Phase Load Switching

To verify the proper operation of the proposed fault detection scheme in the case of load switching, another case study is established in which load 2 (the largest load of CIGRE benchmark) is switched on at $t = 2$ s. For this scenario, the four-wire study microgrid system is adopted and HRFL strategy is implemented for all DERs. As shown in Fig. 10, due to the smooth transition of the inverter current to new condition in this case, d calculated from the output current i_o of DER 2 reaches only 1.2 pu and does not exceed its threshold. Table V shows that for the same load switching event in three-wire configuration, d calculated from i_L^{ref} (obtained from the auxiliary voltage control implemented in NARF) increases only to 1.4 pu which shows that the proposed fault detection scheme has no malfunction during a load switching for both three- and four-wire configurations.
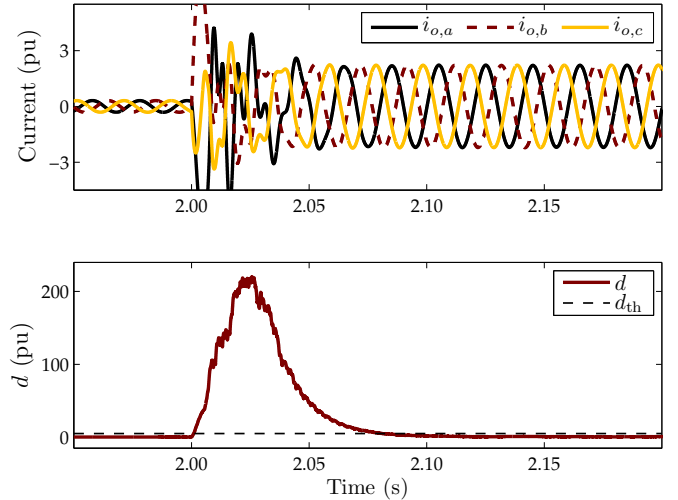

Fig. 9. Output current and d calculated for DER 5 of the study microgrid during an a-b-c-g fault. DERs are three-leg and equipped with the LL strategy.

VII. CONCLUSION

The motivation of this paper is to study the effect of inverter topology, current limiting strategy, and adopted reference frame on the performance of fault detection schemes for inverter-interfaced autonomous microgrids. Analysis of two of the most used local fault detection schemes shows that their performance degrades in some fault conditions. The developed fault detection scheme employs the transient monitoring function calculated from the inverter current as a local feature. For the SYRF and STRF cases in three-wire systems, an auxiliary control system implemented in NARF
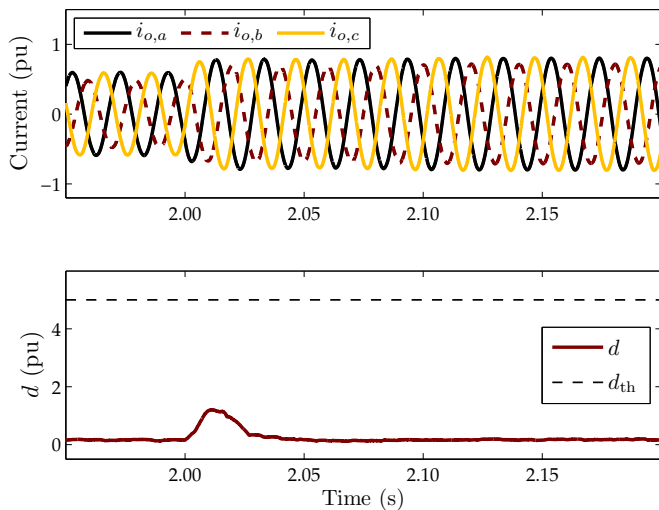
Fig. 10. Output current and d calculated for DER 2 of the study microgrid during a three-phase load switching. DERs are four-leg and equipped with the HRFL strategy.

is developed to increase the ability of the proposed scheme in detecting a single-phase to ground fault. In these cases, the inverter current reference given by the parallel voltage control is employed to calculate TMF. The proposed fault detection scheme does not require communication links and can be implemented in microprocessor-based relays. It can also distinguish a symmetrical/asymmetrical load switching from a fault condition because the former has smooth transition to the new conditions and does not change TMF significantly. Equally importantly, the developed fault detection scheme is effective for both three- and four-leg inverters, all main current limiting strategies, and all reference frames. Several symmetrical and asymmetrical fault scenarios performed on the CIGRE benchmark LV microgrid network verify the effectiveness of the proposed fault detection scheme.

REFERENCES

[1] M. Monfared, S. Golestan, and J. Guerrero, "Analysis, design, and experimental verification of a synchronous reference frame voltage control for single-phase inverters," *IEEE Trans. Ind. Electron.*, vol. 61, no. 1, pp. 258–269, Jan. 2014.

[2] M. Zamani, A. Yazdani, and T. Sidhu, "A communication-assisted protection strategy for inverter-based medium-voltage microgrids," *IEEE Trans. Smart Grid*, vol. 3, no. 4, pp. 2088–2099, Dec. 2012.

[3] M. Yazdanian and A. Mehrizi-Sani, "Distributed control techniques in microgrids," *IEEE Trans. Smart Grid*, vol. 5, no. 6, pp. 2901–2909, Nov. 2014.

[4] M. Zamani, T. Sidhu, and A. Yazdani, "A protection strategy and microprocessor-based relay for low-voltage microgrids," *IEEE Trans. Power Del.*, vol. 26, no. 3, pp. 1873–1883, Jul. 2011.

[5] A. Micallef, M. Apap, C. Spiteri-Staines, and J. M. Guerrero, "Single-phase microgrid with seamless transition capabilities between modes of operation," *IEEE Trans. Smart Grid*, vol. 6, no. 6, pp. 2736–2745, Nov. 2015.

[6] N. Pogaku, M. Prodanovic, and T. Green, "Modeling, analysis and testing of autonomous operation of an inverter-based microgrid," *IEEE Trans. Power Electron.*, vol. 22, no. 2, pp. 613–625, Mar. 2007.

[7] E. Sortomme, S. Venkata, and J. Mitra, "Microgrid protection using communication-assisted digital relays," *IEEE Trans. Power Del.*, vol. 25, no. 4, pp. 2789–2796, Oct. 2010.

[8] B. M. Duong, K. Y. Lien, S. L. Chen, Y. C. Lu, C. M. Chan, and Y. R. Chang, "Investigate dynamic and transient characteristics of microgrid operation and develop a fast-scalable-adaptable algorithm for fault protection system," *Electr. Pow. Syst. Res.*, vol. 120, pp. 214–233, 2015.

[9] T. Loix, T. Wijnhoven, and G. Deconinck, "Protection of microgrids with a high penetration of inverter-coupled energy sources," in *CIGRE/IEEE PES Joint Symp.*, Calgary, Canada, Jul. 2009, pp. 1–6.

[10] I. Sadeghkhani, M. Hamedani Golshan, J. Guerrero, and A. Mehrizi-Sani, "A current limiting strategy to improve fault ride-through of inverter interfaced autonomous microgrids," *IEEE Trans. Smart Grid*, vol. accepted for publication, Jan. 2016.

[11] M. Haj-Ahmed and M. Illindala, "The influence of inverter-based DGs and their controllers on distribution network protection," *IEEE Trans. Ind. Appl.*, vol. 50, no. 4, pp. 2928–2937, Jul. 2014.

[12] E. Casagrande, W. L. Woon, H. Zeineldin, and N. Kan'an, "Data mining approach to fault detection for isolated inverter-based microgrids," *IET Gener. Transm. Distrib.*, vol. 7, no. 7, pp. 745–754, Jul. 2013.

[13] E. Casagrande, W. Woon, H. Zeineldin, and D. Svetinovic, "A differential sequence component protection scheme for microgrids with inverter-based distributed generators," *IEEE Trans. Smart Grid*, vol. 5, no. 1, pp. 29–37, Jan. 2014.

[14] H. Al-Nasseri and M. Redfern, "A new voltage based relay scheme to protect micro-grids dominated by embedded generation using solid state converters," in *19th Int. Conf. Electricity Distrib.*, Vienna, May 2007.

[15] S. M. Brahma, "Fault location in power distribution system with penetration of distributed generation," *IEEE Trans. Power Del.*, vol. 26, no. 3, pp. 1545–1553, Jul. 2011.

[16] H. Al-Nasseri and M. A. Redfern, "Harmonics content based protection scheme for micro-grids dominated by solid state converters," in *12th Int. Middle-East Power Syst. Conf., MEPCON*, Aswan, Mar. 2008, pp. 50–56.

[17] M. Petit, X. L. Pivert, and L. Garcia-Santander, "Directional relays without voltage sensors for distribution networks with distributed generation: Use of symmetrical components," *Electr. Pow. Syst. Res.*, vol. 80, no. 10, pp. 1222–1228, 2010.

[18] S. Ndjaba, G. T. Machnida, M. Nthontho, S. Chowdhury, S. P. Chowdhury, and N. Mbuli, "Modeling and simulation of fault detection methods for power electronic interfaced microgrids," in *47th Int. Universities Power Engineering Conf. (UPEC)*, London, Sep. 2012.

[19] H. Nikkhajoei and R. Lasseter, "Microgrid fault protection based on symmetrical and differential current components," Public Interest Energy Research, California Energy Commission, Tech. Rep., 2006.

[20] S. Kar and S. Samantaray, "Time-frequency transform-based differential scheme for microgrid protection," *IET Gener. Transm. Distrib.*, vol. 8, no. 2, pp. 310–320, Feb. 2014.

[21] W. Huang, T. Nengling, X. Zheng, C. Fan, X. Yang, and B. J. Kirby, "An impedance protection scheme for feeders of active distribution networks," *IEEE Trans. Power Del.*, vol. 29, no. 4, pp. 1591–1602, Aug. 2014.

[22] D. Olivares, A. Mehrizi-Sani, A. Etemadi, C. Canizares, R. Iravani, M. Kazerani, A. Hajimiragha, O. Gomis-Bellmunt, M. Saeedifard, R. Palma-Behnke, G. Jimenez-Estevez, and N. Hatziargyriou, "Trends in microgrid control," *IEEE Trans. Smart Grid*, vol. 5, no. 4, pp. 1905–1919, Jul. 2014.

[23] A. Mehrizi-Sani and R. Iravani, "Potential-function based control of a microgrid in islanded and grid-connected modes," *IEEE Trans. Power Syst.*, vol. 25, no. 4, pp. 1883–1891, Nov. 2010.

[24] N. Bottrell and T. Green, "Comparison of current-limiting strategies during fault ride-through of inverters to prevent latch-up and wind-up," *IEEE Trans. Power Electron.*, vol. 29, no. 7, pp. 3786–3797, Jul. 2014.

[25] M. Baran and I. El-Markaby, "Fault analysis on distribution feeders with distributed generators," *IEEE Trans. Power Syst.*, vol. 20, no. 4, pp. 1757–1764, Nov. 2005.

[26] C. Plet, M. Graovac, T. Green, and R. Iravani, "Fault response of grid-connected inverter dominated networks," in *IEEE Power and Energy Society General Meeting*, Minneapolis, MN, Jul. 2010.

[27] "IEEE recommended practice and requirements for harmonic control in electric power systems," *IEEE Std 519-2014 (Revision of IEEE Std 519-1992)*, pp. 1–29, Jun. 2014.

[28] A. G. Phadke and J. S. Thorp, *Computer Relaying for Power Systems*. John Wiley & Sons, 2009.

[29] S. Papathanassiou, N. Hatziargyriou, and K. Strunz, "A benchmark low voltage microgrid network," in *CIGRE Symp. on Power systems with Dispersed Generation*, Athens, Greece, Apr. 2005.

[30] J. Peas Lopes, C. Moreira, and A. Madureira, "Defining control strategies for microgrids islanded operation," *IEEE Trans. Power Syst.*, vol. 21, no. 2, pp. 916–924, May 2006.

Iman Sadeghkhani (GSM'15) received the B.Sc. (Hons.) degree in electrical engineering from the Islamic Azad University of Najafabad, Najafabad, Iran, in 2007, and the M.Sc. (Hons.) degree in electrical engineering from the University of Kashan, Kashan, Iran, in 2009. He is currently pursuing the Ph.D. degree in electrical engineering with the Isfahan University of Technology, Isfahan, Iran.

His areas of interest include control and management of microgrids, power electronics interfaces for distributed generation, and power system protection.

Mr. Sadeghkhani was a recipient of the University of Kashan Award for Distinguished Research in 2010 and the Exceptional Reviewer Award from the IEEE TRANSACTIONS ON POWER DELIVERY in 2014.

Mohamad Esmail Hamedani Golshan was born in Isfahan, Iran, in 1964. He received the B.Sc. degree from the Isfahan University of Technology, Isfahan, Iran, in 1987; the M.Sc. degree from the Sharif University of Technology, Tehran, in 1990; and the Ph.D. degree from the Isfahan University of Technology, Isfahan, Iran, in 1998, all in electrical engineering.

He is currently a Professor with the Department of Electrical and Computer Engineering, Isfahan University of Technology. His major research interests are power system analysis, power system dynamics, power quality, dispersed generation, flexible ac transmission systems and custom power, and load modeling special arc furnace modeling.

Ali Mehrizi-Sani (S'05–GS'08–M'12–SM'15) received the B.Sc. degrees in electrical engineering and petroleum engineering from Sharif University of Technology, Tehran, Iran, both in 2005. He received the Ph.D. degree from the University of Toronto, Toronto, ON, Canada, both in electrical engineering, in 2007 and 2011.

He is currently an Assistant Professor at Washington State University, Pullman, WA, USA. He was a Visiting Professor at Graz University of Technology, Graz, Austria, in Nov. 2014 and Jan. 2016. His areas of interest include power system applications of power electronics and integration of renewable energy resources.

Dr. Mehrizi-Sani is an editor of IEEE TRANSACTIONS ON POWER SYSTEMS, IEEE TRANSACTIONS ON POWER DELIVERY, and IEEE TRANSACTIONS ON ENERGY CONVERSION. He is the Chair of IEEE TASK FORCE ON DYNAMIC SYSTEM EQUIVALENTS and the Secretary of the CIGRE Working Group C4.34 on Application of PMUs for Monitoring Power System Dynamic Performance. He received WSU VCEA Reid Miller Excellence in Teaching Award in 2016. He is a recipient of the NSERC Postdoctoral Fellowship in 2011. He was a Connaught Scholar at the University of Toronto. He received the Dennis Woodford prize for his M.Sc. thesis.

Josep M. Guerrero (S'01–M'04–SM'08–FM'15) received the B.S. degree in telecommunications engineering, the M.S. degree in electronics engineering, and the Ph.D. degree in power electronics from the Technical University of Catalonia, Barcelona, in 1997, 2000 and 2003, respectively. Since 2011, he has been a Full Professor with the Department of Energy Technology, Aalborg University, Denmark, where he is responsible for the Microgrid Research Program. From 2012 he is a guest Professor at the Chinese Academy of Science and the Nanjing University of Aeronautics and Astronautics; from 2014 he is chair Professor in Shandong University; and from 2015 he is a distinguished guest Professor in Hunan University.

His research interests is oriented to different microgrid aspects, including power electronics, distributed energy-storage systems, hierarchical and cooperative control, energy management systems, and optimization of microgrids and islanded minigrids; recently specially focused on maritime microgrids for electrical ships, vessels, ferries and seaports. Prof. Guerrero is an Associate Editor for the IEEE TRANSACTIONS ON POWER ELECTRONICS, the IEEE TRANSACTIONS ON INDUSTRIAL ELECTRONICS, and the IEEE INDUSTRIAL ELECTRONICS MAGAZINE, and an Editor for the IEEE TRANSACTIONS ON SMART GRID and IEEE TRANSACTIONS ON ENERGY CONVERSION. He has been Guest Editor of the IEEE TRANSACTIONS ON POWER ELECTRONICS Special Issues: Power Electronics for Wind Energy Conversion and Power Electronics for Microgrids; the IEEE TRANSACTIONS ON INDUSTRIAL ELECTRONICS Special Sections: Uninterruptible Power Supplies systems, Renewable Energy Systems, Distributed Generation and Microgrids, and Industrial Applications and Implementation Issues of the Kalman Filter; and the IEEE TRANSACTIONS ON SMART GRID Special Issue on Smart DC Distribution Systems. He was the chair of the Renewable Energy Systems Technical Committee of the IEEE Industrial Electronics Society. He received the best paper award of the IEEE TRANSACTIONS ON ENERGY CONVERSION for the period 2014-2015. In 2014 and 2015 he was awarded by Thomson Reuters as Highly Cited Researcher, and in 2015 he was elevated as IEEE Fellow for his contributions on "distributed power systems and microgrids."

www.microgrids.et.aau.dk

Abbas Ketabi received the B.Sc. and M.Sc. degrees in electrical engineering from the Department of Electrical Engineering, Sharif University of Technology, Tehran, Iran, in 1994 and 1996, respectively. He received the Ph.D. degree in electrical engineering jointly from Sharif University of Technology and the Institut National Polytechnique de Grenoble (Grenoble Institute of Technology), Grenoble, France, in 2001. Since then, he has been at the University of Kashan, Department of Electrical Engineering, where he is currently an Associate Professor. He has published more than 70 technical papers and 4 books. He is manager and editor of "Energy: Engineering and Management" journal. Dr. ketabi was the recipient the University of Kashan Award for Distinguished Teaching and research. His research interests include power system restoration, smart grids, renewable energy, and evolutionary computation.